

Temperature dependent partitioning mechanisms and its associated microstructural evolution in a CMnSiAl quenching and partitioning (Q&P) steel

N. Maheswari^{a,*}, Murugaiyan Amirthalingam^a, Alexander Schwedt^b, Heinz Günter Brokmeier^c, Norbert Schell^d, Joachim Mayer^b, K.C. Hari Kumar^a and S.Sankaran^a

^aDepartment of Metallurgical and Materials Engineering, IIT Madras, Chennai, India

^bCentral Facility for Electron Microscopy (GFE), RWTH Aachen University, Ahornstr. 55, D- 52074 Aachen, Germany

^cInstitute of Materials Science and Engineering, Clausthal University of Technology Agricolastrasse 6, D-38678 Clausthal-Zellerfeld, Germany

^dGerman Engineering Materials Science Center at DESY, Helmholtz-Zentrum Geesthacht, D-22607 Hamburg, Germany

ARTICLE INFO

Keywords:


Quenching and partitioning (Q&P) steels
Interface migration
Carbon partitioning mechanism
Isothermal martensite
Distorted BCC or pseudo tetragonal martensite

ABSTRACT

The effect of temperature ($350^{\circ}\text{C} < M_s < 450^{\circ}\text{C}$) on the partitioning mechanisms and the final microstructure evolution in a CMnSiAl quenching and partitioning (Q&P) steel was investigated. The microstructure of both the Q&P specimens, comprised of distorted BCC or pseudo tetragonal martensite structure with two different characteristics namely (i) tempered or carbon depleted martensite that formed during initial quenching ($M_f < 240^{\circ}\text{C} < M_s$) and partitioning step and (ii) carbon enriched fresh martensite that formed after partitioning step and final quenching (RT) together with blocky and inter-lath films of retained austenite. In addition, packets of M/A constituents were observed in Q&P-350-1min specimen and some traces of carbide and plate martensite were observed in Q&P-450-1min specimen. The increase in partitioning temperature led to nearly 2% increase in the amount of retained austenite (both blocky and inter-lath) with increased carbon content of 0.27 wt.%. Along with carbon partitioning, slight interface mobility/isothermal martensite formation was also observed in the case of specimen partitioned at 350°C , whereas tempering effect was predominantly seen in the case of specimen partitioned at 450°C . Irrespective of the partitioning temperature, the amount of carbon required to stabilize the retained austenite at RT was found to be about 1.15 wt.% and was confirmed through APT analysis.

1. Introduction

Quenching and partitioning steels are a class of advanced high-strength steels which are candidate materials for light-weighting of automotive steel components [1]. These steels contain multiphase (ferrite, bainite, retained austenite and martensite) microstructures with increased thermal and mechanical stability of retained austenite as compared to conventional retained austenite containing transformation induced plasticity (TRIP) steels. This increase in stability of retained austenite is achieved by the preferential partitioning of carbon from supersaturated martensite upon reheating followed by quenching from austenitization temperature. This heat treatment to enhance the stability of retained austenite, known as quenching and partitioning (Q&P), was first reported by Speer, *et al.* [1]. The Q&P process has been subsequently explored to obtain steels with required volume fraction of retained austenite with a combination of high strength (UTS of >1000 MPa) and uniform elongation (20 to 35 %) [2, 3, 4, 5, 6]. Efforts were made to understand the mechanism of carbon partitioning from the supersaturated martensite to austenite through experiments as well as through numerical modelling [7, 8, 9, 10, 11, 12, 13, 14]. In these studies, partitioning temperatures are generally chosen either below or above martensite start (M_s) temperature upon quenching directly from full or partial austenitization temperature. Also, it is believed that the carbon partitioning takes place under constrained carbon equilibrium (CCE) from carbon supersaturated martensite to austenite through an immobile interface [1, 6, 15]. However, Santofimia *et al.*, [7] has verified the low mobility of martensite-austenite interface with simulation and reported the same as the cause for the expansion observed during partitioning treatment in the dilatometer measurement. Recently, with theoretical as well as experimental investigation, Dai *et al.* [14], have predicted through local equilibrium (LE)

 maheswarims06@gmail.com (N. Maheswari)
ORCID(s):

model in two Fe-C-Mn-Si steels that, based on the alloy composition, quenching temperature and partitioning temperature, the austenite-martensite interface could migrate during the Q&P process. Speer *et al.* [8], have done a critical assessment on the reported works on various Q&P steels and consolidated the possible mechanisms involved during partitioning as follows. The specimen expansion during partitioning with dilatometric analysis at low (below M_S) partitioning temperatures may correspond to (i) low interface mobility and little migration, (ii) bainitic growth, and/or (iii) isothermal martensite formation. Whereas, the dilatometric contractions observed at higher (above M_S) partitioning temperatures may be due to (i) reduced ferrite growth, (ii) austenite growth, and/or (iii) tempering in martensite. But still the ambiguity continues and the proper reason for the Q&P microstructure evolution mechanism is not very clear.

Also, there is not much detailed reports in the literature on the lattice parameter variation in austenite prior to transformation as function of carbon content. With time-resolved Synchrotron X-ray diffraction technique, Babu, *et al.* [16], have observed the peak splitting corresponds to carbon-rich and carbon-poor regions in the austenite during initial stage of isothermal holding and it disappears as the bainitic transformation continued in a Fe-C-Si-Mn-Mo-Cr-V-Al-P-S steel. Similarly, Takahama *et al.* [9], have found a strong inhomogeneous distribution of carbon content in austenite grains at short partitioning times by using phase field simulation on a CMnSiAlP steel. They expect it to vary the mechanical stability of individual austenite during deformation. Ebner *et al.* [17], have observed the change in c/a ratio (tetragonality) of BCT (Body centered tetragonal) phase w.r.t partitioning time in a CSiMn steel. They have also calculated the change in amount of fresh martensite, tempered martensite, bainite and the austenite carbon content during 1-step and 2-step Q&P treatments by only based on the in-situ synchrotron X-ray diffraction [17]. The inhomogeneity of carbon in austenite during austenitization and during partitioning could affect the carbon partitioning mechanism and the phase transformation between martensite- austenite. Thus, it is very important not only to study the lattice parameter variation in austenite and martensite during various stages of Q&P treatment but also to carryout detailed characterization involving quantification of microstructural evolution and elemental partitioning are necessary in a typical Q&P treatment.

Therefore, in this work, using the advanced characterization techniques such as atom probe tomography (APT) and high energy synchrotron X-ray diffraction (HEXRD), the local interface carbon content and volume fraction of austenite were quantified as a function of partitioning temperatures. The dilatometric analysis during Q&P process was studied by using Gleeble thermo-mechanical simulator to understand the dilation characteristics and its influence on the microstructural evolution that happens during partitioning. In addition, an attempt is made with the correlative TEM and EBSD microstructural data along with thermodynamic calculation to arrive at a clear mechanism of partitioning in the Q&P steels.

2. Experimental Procedure

2.1. Quenching and partitioning process

The steel of desired composition was selected based on the physical metallurgical aspects and the alloy selection is explained in detail elsewhere [11]. The selected steel was processed through induction melting and casted in the form of billets. The composition of as-cast billet was verified with inductively coupled plasma optical emission spectrometer (ICP- OES) as 0.26 C-1.57 Mn- 1.06 Si-0.98 Al (in wt.%). The martensite start (M_S) temperature of the steel was calculated using an empirical formula (Eq.3) [5], which is 403°C. Fig.1 shows the quenching and partitioning (Q&P) heat treatment schedule: the steel was fully austenitized at 1000°C for 1 h to get a homogeneous microstructure, quenched at 240°C ($M_f < 240^\circ\text{C} < M_S$) in a salt bath furnace for 20 s, partitioned below M_S , at 350°C for 1 minute (Q&P 350-1min specimen) [11] and partitioned above M_S , at 450°C for 1 minute (Q&P 450-1min specimen). The theoretical volume fraction of austenite as a function of cooling from M_S was calculated using Koistinen-Marburger (K-M) relation [19]. Based on the K-M approach, the optimum quenching temperature of 240°C was selected to retain nearly 15 vol.% austenite after partitioning process [19].

2.2. Synchrotron X-ray diffraction

The high energy synchrotron X-ray diffraction (HEXRD) has higher resolution due to its finer beam size, shorter wavelength and high penetration depth as compared to conventional X- ray diffraction. Therefore, it is one of the best suitable tools to determine the change in crystallographic characteristics such as, lattice parameter, d -spacing, microstrain, etc., of phases present in Q&P specimens [20]. The HEXRD measurements on the Q&P specimens were carried out in the high energy beam line HEMS P07B at DESY (Deutsches Elektronen-Synchrotron), Hamburg, Germany. The calibration was done with LaB₆ specimen and the high energy beam with wavelength of 0.14235 Å was

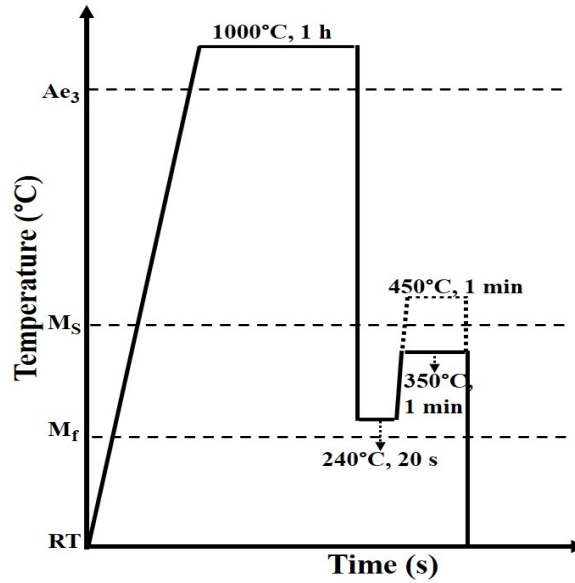


Figure 1: Q&P heat treatment schedule: A_{e3} – upper critical temperature calculated using Thermo-Calc [18]; M_s -martensite start temperature calculated using an empirical formula [5]; M_f -martensite finish temperature; RT- room temperature.

used for the measurements. The sample was not rotated (0°), counting time used was 10 s/image with slit system of $0.5 \text{ mm} \times 0.5 \text{ mm}$. The Q&P steel specimens with size of $10 \times 5 \times 5 \text{ mm}^3$ (length \times width \times thickness) were used for the HEXRD studies in Bragg reflection mode and the diffracted data was recorded on a 2D Perkin Elmer XRD 1622 detector. The use of complete Debye- Scherrer rings leads on one hand to excellent statistics and on the other on texture free results [21].

The Rietveld refinement of the XRD data (for the 2θ range from 3.5 to 14°) was done by using MAUD software to calculate the volume fraction and lattice parameter of martensite and retained austenite. The amount of carbon that is present in austenite was calculated using the lattice parameter value obtained from Rietveld refinement (Table 1) and by substituting it in the following empirical equation 1 [5].

$$a_\gamma(\text{\AA}) = 3.556 + 0.0453w_C + 0.00095w_{Mn} + 0.0056w_{Al} \quad (1)$$

where, w -is the composition of alloying elements in wt.%.

2.3. EBSD analysis

The microstructural analysis was carried out by electron back- scatter diffraction (EBSD) to confirm the presence of retained austenite and lath martensite on the heat-treated Q&P specimens. The specimens were prepared by electro polishing with A2- electrolyte (ethanol-720 ml, butoxy ethanol-110 ml, distilled water-80 ml, perchloric acid-78 ml). The measurements were performed using a scanning electron microscope (JEOL JSM 7000F, JEOL Ltd., Tokyo, Japan) with 20 kV applied voltage, on an area of interest of $150 \times 300 \mu\text{m}$ on the Q&P treated steel with a step size of 100 nm. The measured EBSD data were post-processed with TSL - OIM analysis software. All evaluations relying on the correct indexing were restricted to confidence index (CI) > 0.1 .

2.4. Transmission electron microscopy

Q&P treated specimens were analyzed in detail by transmission electron microscopy (TEM), upon identifying regions containing lath martensite, inter-lath austenite and retained austenite blocks on the prior austenite grain boundaries. For TEM studies, the cross-sectional lamellae were prepared at the RoI using FEI Helios NanoLab 400S focused ion beam (FIB) system. Selected area electron diffraction, bright and dark field imaging were performed using FEI Tecnai F20, with an operating voltage of 200 kV.

2.5. Thermomechanical simulator

The thermal cycles used for Q&P heat treatment (Fig.1) were also physically simulated in a dilatometer attached with Gleeble 3800 thermo-mechanical simulator (i) to measure the M_S and M_f temperatures and (ii) to measure the relative length change during partitioning in Q&P specimens. The standard ISO quench round bar (6 mm \times 6 mm length, 10 mm width) specimens for dilatometry measurement were machined from the as-cast billet. Using a heating rate of 5°C min^{-1} , specimens were heated to 1000°C and austenitized for 5 min. Subsequently, the specimens were quenched with a cooling rate of 120°C s^{-1} to room temperature and, M_S and M_f temperatures were identified from the dilatometry data. For Q&P process simulation, the following steps were followed. (i) with heating rate of 5°C min^{-1} , the specimens were austenitized at 1000°C for 5 min; (ii) quenched to 240°C with a cooling rate of 120°C s^{-1} ; (iii) reheated with heating rate of 5°C min^{-1} to the partitioning temperature of 350°C (below M_S) and 450°C (above M_S) and (iv) finally water quenched to room temperature with a cooling rate of 120°C s^{-1} .

2.6. Atom probe tomography

The elemental distribution between the martensite and austenite along the interface was investigated on the Q&P specimens in order to identify the partitioning effect, using atom probe tomography (APT). The specimens for APT studies were prepared using a dual-beam FIB machine (FEI Helios Nanolab 600). The APT measurements were performed with a local electrode atom probe with the tip temperature of about 60 K in APT- LEAPTM 3000X HR (Cameca Instruments) machine. The data obtained was post processed by using the Cameca -IVAS software to plot the elemental composition w.r.t distance of the analyzed region.

3. Results

3.1. Synchrotron X-ray diffraction analysis

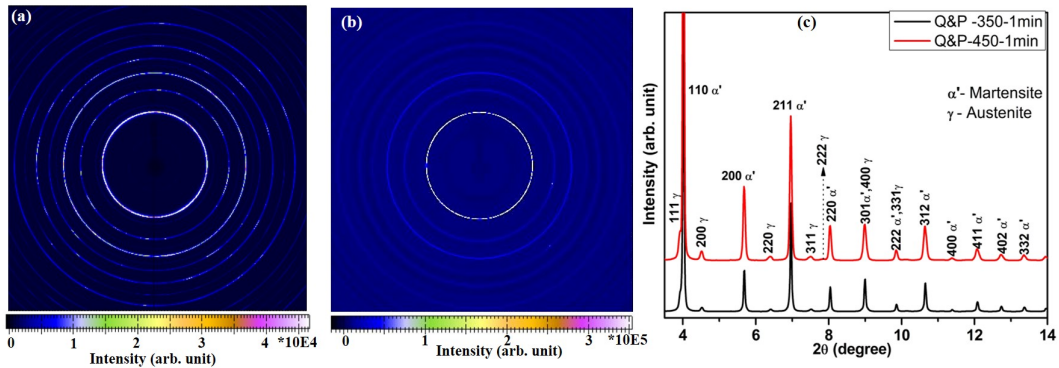


Figure 2: (a, b) 2-D Synchrotron X-ray diffraction pattern showing the Debye-Scherrer rings of martensite and austenite and (c) 1-D integrated pattern from (a, b) showing the intensity versus 2θ confirming the presence of martensite (α') and austenite (γ) peaks in Q&P-350-1min and Q&P- 450-1min specimen, respectively.

The 2-D Debye-Scherrer rings recorded from the HEXRD on the two Q&P specimens are shown in Fig.2a and 2b. Fig.2c represents the 1-D diffraction pattern that was integrated from the intensities of the Debye-Scherrer rings (Fig.2a and 2b) of the (Q&P-350-1min and Q&P-450-1min) partitioned specimens by using the FIT2D software. The pattern has confirmed the presence of martensite and retained austenite and the corresponding peaks are marked in Fig.2c for both below M_S (Q&P-350-1min) and above M_S (Q&P-450-1min) partitioned specimens.

In order to reveal the extent of tetragonality of martensite in both the Q&P specimens (with low carbon in the alloy composition), the variation in d-spacing was calculated with respect to azimuth angle (of Debye-Scherrer rings) by using FIT2D software. Fig.3 shows the non-uniform intensity distribution that indicates the variation in d-spacing of individual BCC/BCT (110, 200 and 211) reflections with respect to azimuth angle (0 - 360°) of Debye-Scherrer rings (Fig.2a and 2b) for Q&P-350-1min and Q&P-450-1min specimen. The results are clearly revealing the change in d-spacing in all the reflections w.r.t azimuth angle in both the Q&P specimens, which is evident for the distortion in the martensite lattice. Also, from the lattice parameter calculation using Rietveld refinement method (Fig.2c), a

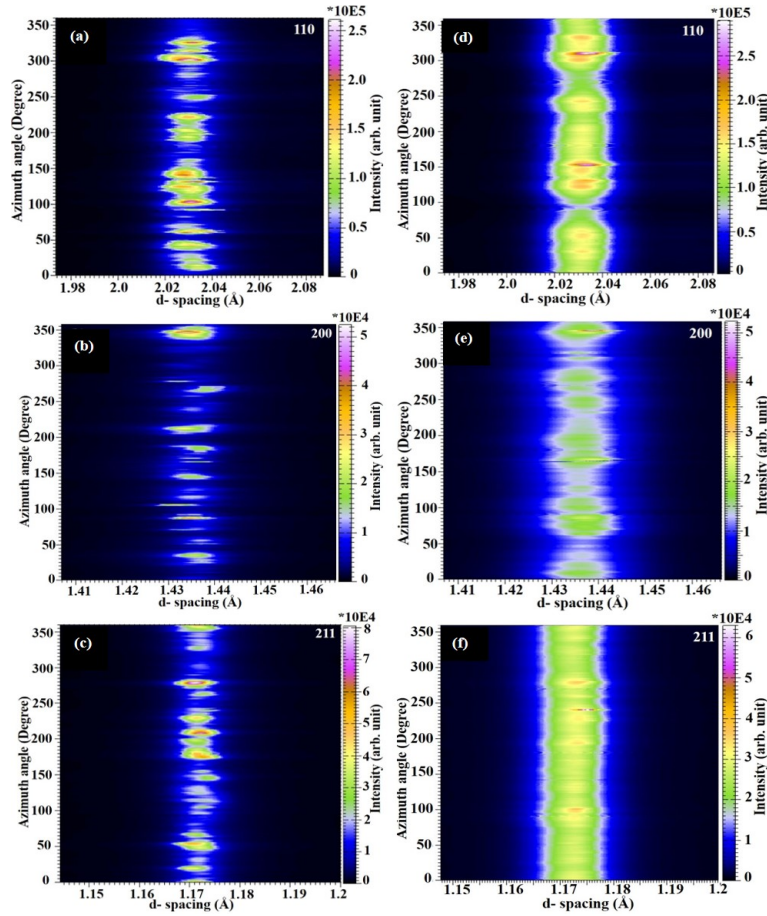


Figure 3: showing the non-uniform intensity distribution that indicates the variation in d-spacing of 110, 200, 211 martensite plane reflections with respect to azimuth angle of the Debye-Scherrer rings, (a to c) in Q&P-350-1min and (d to f) in Q&P-450-1min specimen, respectively.

distortion in martensite lattice was observed and the c/a ratio was 1.003 and 1.006 in Q&P-350-1min and Q&P-450-1min specimens, respectively (Table 1). This confirms that the martensite that are present in these Q&P specimens has distorted body centered cubic (BCC) or pseudo- body centered tetragonal (BCT) crystal structure and not a complete BCC or BCT structure since the carbon content is low (0.25 wt.%) in these specimens. The increase in peak broadening (Fig.2c and Fig.3d-f) that was observed in Q&P-450-1min specimen possibly due to the reduction in martensitic lath size as observed from EBSD analysis (Fig.4), as compared to Q&P-350-1min specimen. The broadening could also be due to the overlapping of two fine martensitic laths with different lattice parameter and carbon content in it as reported by Garcia-Mateo *et al.* [22]. The Q&P specimens that were partitioned above M_S temperature (Q&P-450-1min), has showed slightly more volume percent of retained austenite (7 ± 0.38 %) and contained more amount of carbon in it (1.04 wt.%) as compared to the specimen partitioned at below M_S temperature (Q&P-350-1min) which has 5 ± 0.78 % of retained austenite and contained 0.77 wt.% of carbon (Table 1) in it. The volume percent of austenite that got retained with the Q&P specimens are slightly more (2-4 vol. % increase) than the water quenched (WQ) steel with 3 vol. % of retained austenite and with 3.9 vol. % of retained austenite in the steel quenched at 240°C (which will be published elsewhere).

3.2. EBSD analysis

The EBSD IQ map (Fig.4c, g) and IPF map (Fig.4a, e) of Q&P-350-1min and Q&P-450-1min specimen has shown the presence of martensitic laths grouped as set of packets. These lath packets have organized within a colony and each colony has been separated from the neighboring colonies by the prior austenite grain boundaries (Fig.4). In both Q&P

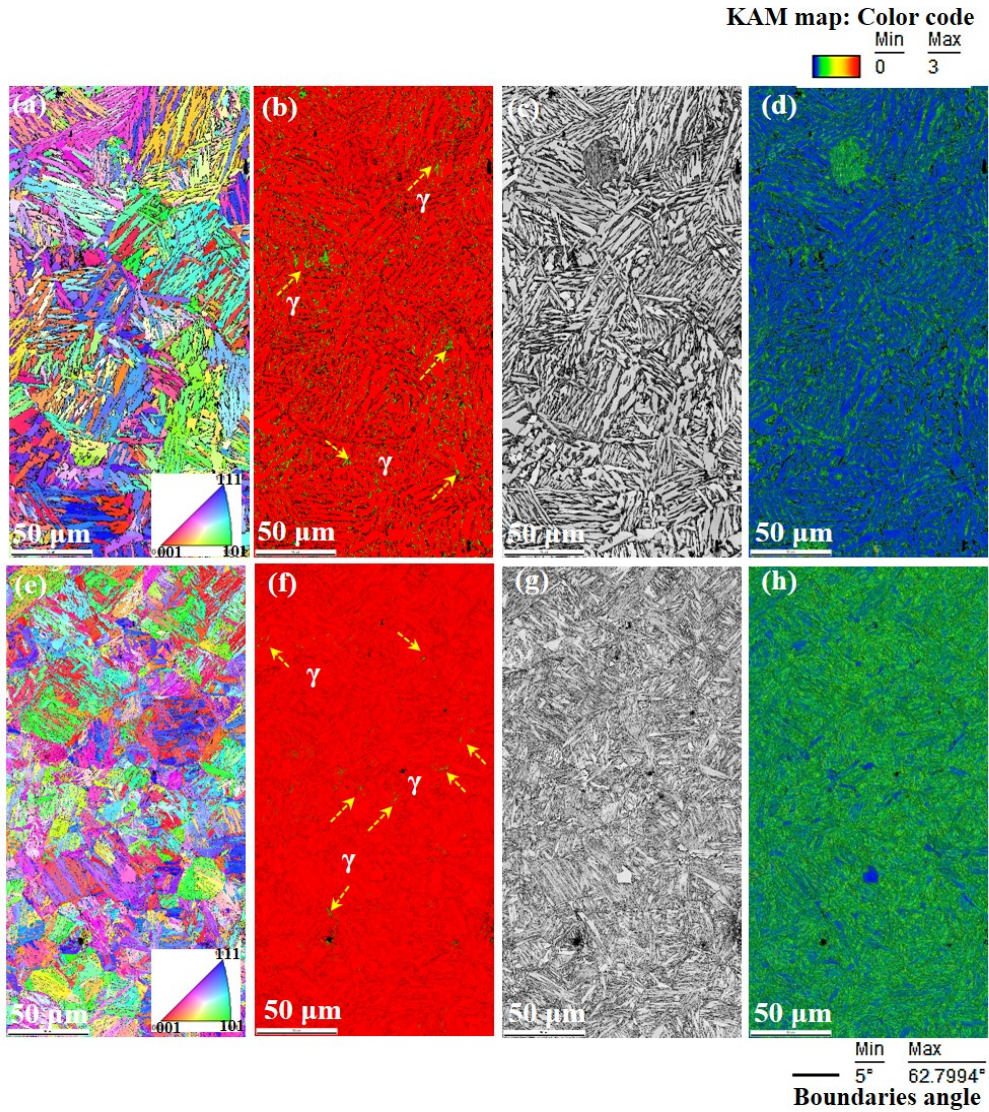


Figure 4: (a,e) EBSD inverse pole figure (IPF) maps showing different orientation of martensitic laths; (b,f) represents the phase map (green-retained austenite (γ), red-martensite); (c,g) image quality (IQ) map and (d,h) Kernel Average Misorientation (KAM) distribution map for nearest neighbour of 100 nm distance (where blue color represents the region with lower misorientation and green represents the region with higher misorientation angle) in Q&P-350-1min and Q&P-450-1min specimen, respectively.

specimens, two different characteristics of martensite are found: one showing high IQ and low KAM, pointing to a comparatively low dislocation density and low strain, and another one showing low IQ and high KAM pointing to a high dislocation density and high strains.

The phase maps (Fig.4b and f) have confirmed the presence of blocky austenite grains in both the Q&P-350-1min and Q&P-450-1min specimens. Some of the thin austenite films that are present in between martensitic laths were also observed in below M_S (Q&P-350-1min) partitioned specimen as in Fig.4b. Whereas, the same was not observed in above M_S (Q&P-450-1min) partitioned specimen as the microstructure is too fine, however, TEM analysis could reveal the inter-lath austenite films which is explained in following Section 3.4.

The misorientation angle plot (Fig.5a and 5b) confirms the austenite misorientation angle of 45° and martensite

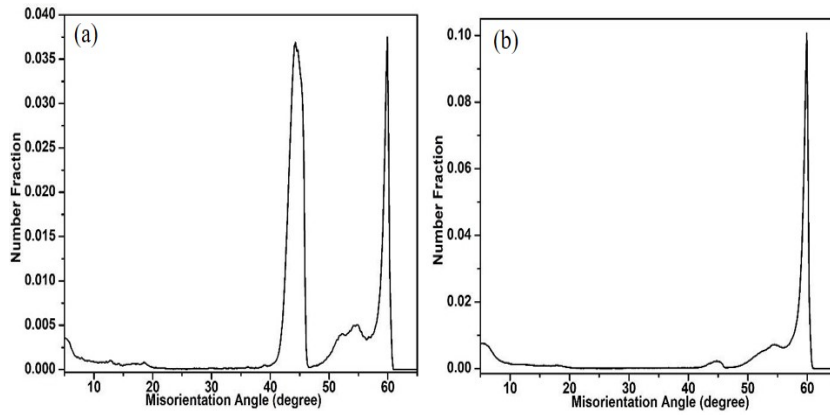


Figure 5: misorientation angle plot in (a) Q&P-350-1min and (b) Q&P-450-1min specimen, respectively.

with corresponding misorientation angles of 55-60° (between the packets and colony) and 5-10° between sub blocks, respectively [23, 24]. The peak intensity at 45° is more in Q&P-350-1min specimen, since more martensite- austenite boundaries are present (as in phase map) in it as compared to Q&P-450-1min specimen.

3.3. FIB specimen preparation for TEM analysis

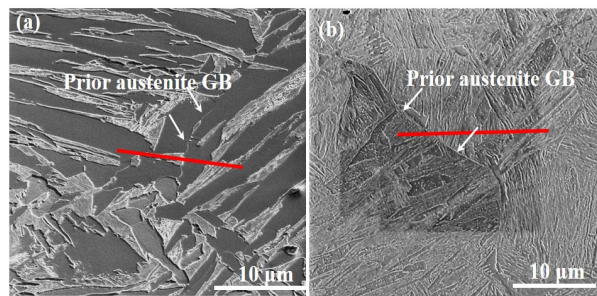


Figure 6: (a, b) SE images showing the presence of lath martensite and the prior austenite grain boundaries. The region of interest (RoI) chosen for FIB milling to prepare TEM lamella is marked in red line in Q&P-350-1min and Q&P-450-1min specimens, respectively.

The specimens for TEM analysis were prepared by using FIB technique and the region of interest (RoI) is marked by red lines in Fig.6a and 6b for the Q&P-350-1min and Q&P-450-1min specimens, respectively. The RoI was selected based on the EBSD- IQ and phase map, where retained austenite was present with the martensite laths along the prior austenite grain boundary in both the partitioned specimens. The specimens were thinned down along the thickness direction.

3.4. TEM analysis

The TEM micrograph of Q&P-350-1min specimen is shown in Fig.7. The bright field micrograph (Fig.7a and b) shows the presence of martensitic laths and martensite-austenite (M/A) constituents. The SAD pattern analysis (Fig. 7c) reveals that the $[\bar{1}12]$ and $[\bar{1}10]$ zone axes pertain to the martensite matrix and $[\bar{1}13]$ zone axis corresponds to the inter-lath austenite in the M/A constituent. The corresponding dark field micrograph that confirms the presence of inter-lath austenite in the M/A constituent is shown in Fig. 7d. The presence of the low carbon martensite lath with dislocations and the packet of martensite-austenite (M/A) constituents are clearly evident in below M_s (Q&P-350-1min) partitioned specimen as shown in Fig.8.

Bright field TEM micrograph of Q&P-450-1min specimen (Fig.9a, b and d) shows the presence of lath martensite, plate martensite, inter-lath austenite. The SAD pattern analysis (Fig.9c and e) shows that the martensite matrix oriented

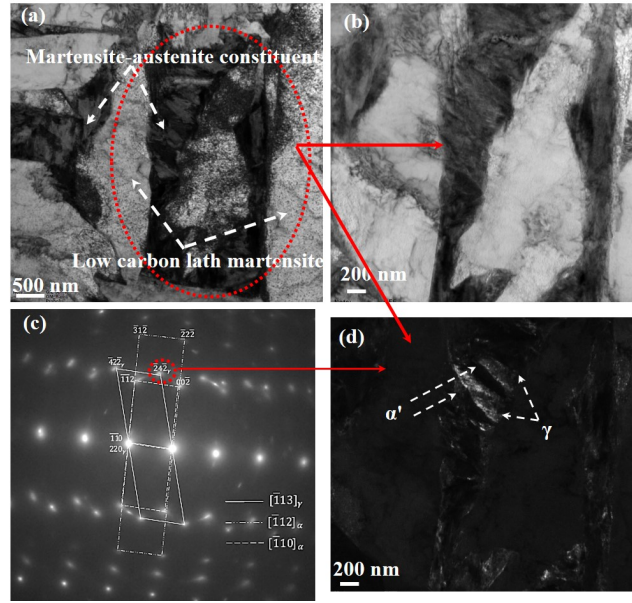


Figure 7: (a) Bright field TEM micrograph reveal the microstructure that contains low carbon lath martensite and martensite-austenite (M/A) constituent; (b and d) higher magnification bright field, dark field micrographs, respectively showing the presence of austenite in the (M/A) constituent and (c) the corresponding SAD pattern from $[113]$ zone axis of austenite, $[112]$ and $[110]$ zone axes of martensite in the Q&P-350-1min specimen.

Table 1
Quantitative microstructural data of Q&P specimens.

		Q&P-350-1 min	Q&P-450-1 min
Volume percent of retained austenite ' V_γ ' (%)		5 ± 0.78	7 ± 0.38
Retained austenite lattice parameter ' a_γ ' (Å)		3.598 ± 0.001	3.61 ± 0.0007
Lattice parameter of martensite (Å)	a	2.865 ± 0.0003	2.865 ± 0.0002
	c	2.873 ± 0.0007	2.882 ± 0.0003
	c/a ratio	1.003	1.006
Carbon content in retained austenite (wt.%)	HEXRD	0.77	1.04
	APT	1.23	1.26
Relative length change (in %) during partitioning		0.024	-0.014

along $[111]$ and $[\bar{1}22]$ zone axis, respectively. The inter-lath austenite has oriented along the $[\bar{1}33]$ zone axis (Fig.9b). Some traces of carbides possibly due to tempering of martensite are noticed and marked in Fig.9a and Fig.10. Since the presence of carbides is highly localised and also its fraction is very small, its corresponding diffracted spot is not visible in the SAD pattern (Fig.9c). Fig.9f confirms the presence of inter-lath austenite from the $[012]$ zone axis as marked in the corresponding SAD pattern (Fig.9e).

The above results from both EBSD and TEM suggest that the microstructure of both the Q&P specimens, comprised of distorted BCC or pseudo tetragonal martensite structure with two different characteristics namely (i) tempered or carbon depleted martensite that formed during initial quenching ($M_f < 240^\circ\text{C} < M_S$) and partitioning step and (ii) carbon enriched fresh martensite that formed after partitioning step and final quenching (RT) together with blocky and inter-lath films of retained austenite.

3.5. Dilatometer analysis

The calculated M_S and M_f temperatures from the dilatometer measurement of water quenched CMnSiAl steel used for the current study are 426°C and 217°C , respectively. From Fig.11a, the volume percent of austenite at 240°C was calculated by using lever rule [25] and the value obtained was 12 %. A slight expansion was observed in the Q&P

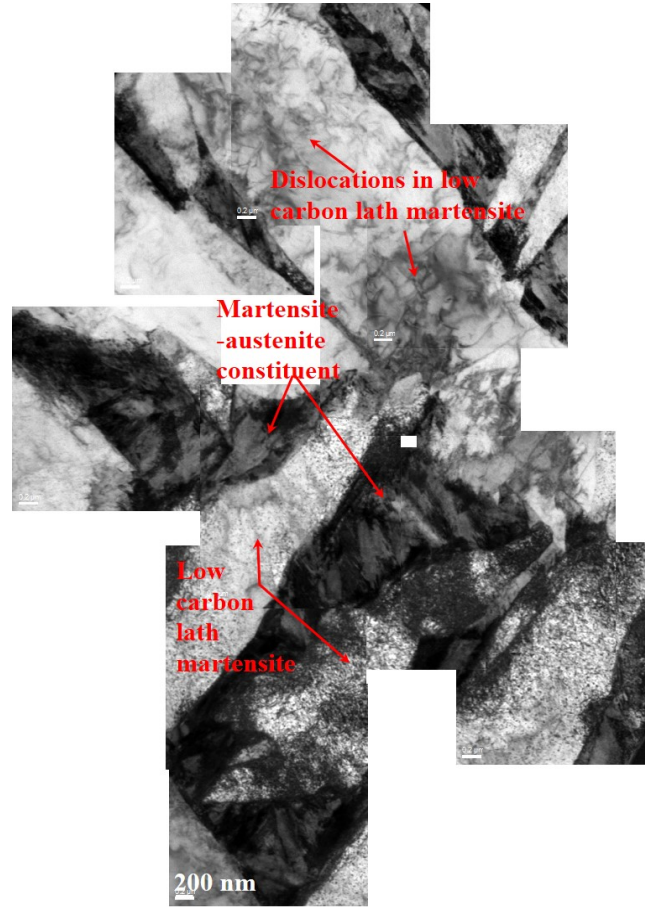


Figure 8: A collage of bright field TEM micrographs displaying region containing colonies of martensite-austenite (M/A) constituents surrounded by low carbon lath martensite containing high dislocation density in Q&P-350-1min specimen.

steel specimen, while holding for 1min at the partitioning temperature of 350°C (Fig.11b) and small but noticeable contraction was noticed in case of 450°C partitioning for 1 min (Fig.11b).

The relative change in length during partitioning treatment (from Fig.11b) in the Q&P steel specimen was measured by using the following equation.

$$\frac{\Delta L}{L_0} = \frac{(L - L_0)}{L_0} \quad (2)$$

where, L_0 is the initial or reference length and L is the instantaneous length of the specimen. The calculated values are listed in Table 1. Nearly, 0.024 % positive expansion was observed in case of Q&P-350-1min specimen, whereas 0.014 % contraction was observed in Q&P-450-1min specimen.

3.6. APT analysis

The elemental distribution maps and iso-surface maps for Q&P-350-1min specimen and Q&P-450-1min specimen are shown in Fig.12 and 13, respectively. From the APT analysis of Q&P-350-1min specimen (Fig.12c), the amount of carbon and manganese measured in austenite was 5.7 at.% (1.23 wt.%) and 2.7 at.%, respectively. In case of Q&P-450-1min specimen (Fig.13c), the carbon and manganese content in austenite was 5.5 at.% (1.26 wt.%) and 3.2 at.%, respectively. The measured carbon content values are much higher than that of the average alloy composition (0.26 wt.% C or 1.2 at.% C). In general, cementite contains 25 at.% of carbon, whereas ϵ -carbide has 25–33 at.% C. Thus, the carbon enriched region analyzed in the Fig.12 and 13 must be the inter-lath austenite (with nearly 6 at.% C). By comparing the measured carbon content from the analysed region with the earlier published results in literature [29]

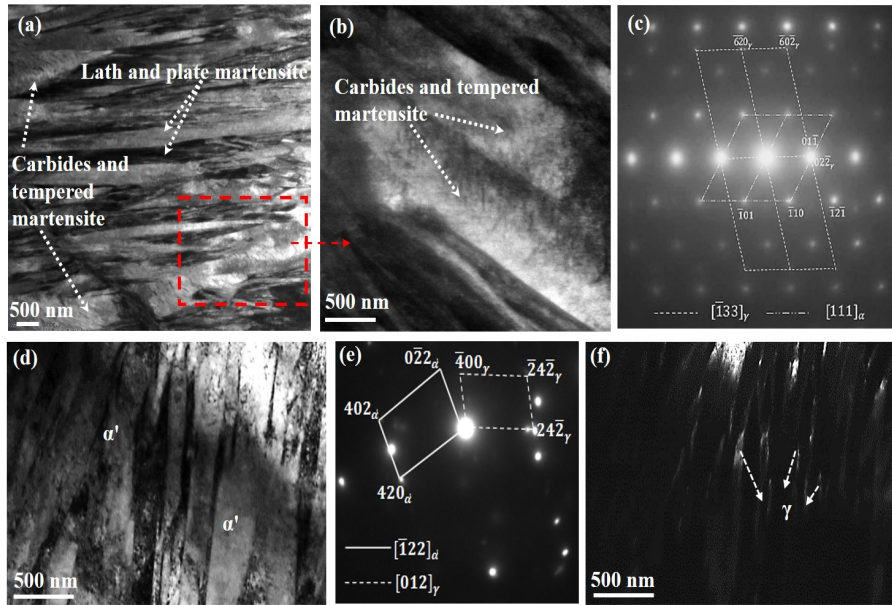


Figure 9: (a,d) Bright field TEM micrograph reveal the microstructure that contains lath and plate martensite and some possible carbides along the tempered lath martensite; (b) the high magnification bright field image of marked area in 'a'; (f) dark field micrograph confirming the presence of inter-lath austenite; and (c and e) the corresponding SAD pattern analysis in the Q&P-450-1min specimen.

and basic physical metallurgical principles, the carbon enriched region is marked as γ and the neighbouring martensite laths are marked as α' in Fig.12c and 13c.

Also, it is clearly evident that a local Mn enrichment exists along with the enrichment of C in austenite as shown in elemental profile taken from cylinder-1 during partitioning at 350 and 450°C for 1min (Fig.12c and 13c respectively). But this Mn enrichment was not observed in all the carbon enriched austenite regions which is evident from the uniform Mn distribution in cylinder-2 (Fig. 12c and 13c) in both the Q&P specimens.

4. Discussion

4.1. Effect of temperature on partitioning mechanism

In both the Q&P specimens that are partitioned at below M_S and above M_S temperature (Q&P- 350-1min and Q&P-450-1min specimen, respectively), the martensite has exhibited the distorted BCC or pseudo-BCT (i.e., partially tetragonal) crystal structure but not a complete BCC/BCT structure, as evident from the HEXRD analysis. Lobodyuk, *et al.*[26] has reported in Fe-C alloys that the martensite has pseudo-tetragonal crystal structure due to the average distortion in the lattice rather than true tetragonal structure. Also, Yuan Lu *et al.* [27] has studied the effect of carbon content on c/a ratio of martensite in low carbon steels with < 0.6 wt.% carbon and reported that martensite exhibits BCT and not complete BCC crystal structure. The increase in partitioning temperature in Q&P-450-1min specimen, has led to the formation of slightly more (2% increase) volume percent of retained austenite with nearly 0.27 wt.% increase in carbon content in it as compared to the Q&P-350-1min specimen (Table 1). In both Q&P specimens, the martensite is evident with two different characteristics: (i) the laths with high IQ and low KAM are expected to be the tempered or partitioned martensite which could have formed during initial intermediate quenching (between M_S and M_f) and relieved the stress via carbon partitioning. (ii) Whereas, the low IQ, high KAM and fine laths are expected to be the martensite that are transformed from carbon enriched austenite (but not stabilized at RT) after partitioning treatment followed by final water quenching (Fig.4). Similar difference in contrast in IQ map and evidence for two type of martensite was reported by Santofimia, *et al.*, in a Q&P treated CMnNiCrSi steel [23]. The presence of blocky and inter-lath film of retained austenite in martensite colonies/packets are evident in both the cases. In addition to lath martensite, the packet of martensite- austenite (M/A) constituents are clearly evident in Q&P-350-1min specimen (Fig.7 and 8). Whereas, in Q&P-450-1min specimen, plate martensite, inter-lath austenite and some localised traces

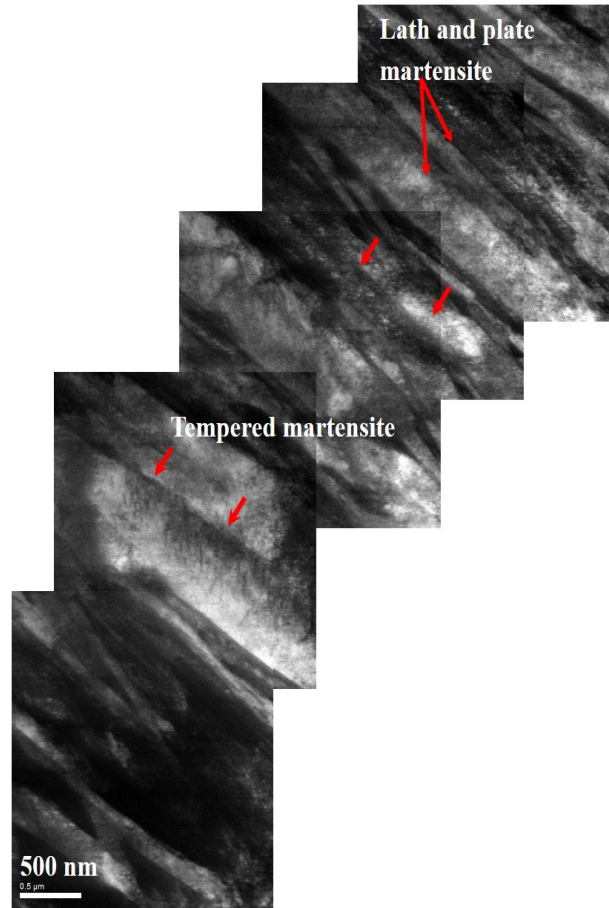


Figure 10: A montage of bright field TEM micrographs displaying the details of lath and plate martensite after partitioning at 450° for 1min. A signature of decomposition of the laths is noticed as result of tempering in Q&P-450-1min specimen.

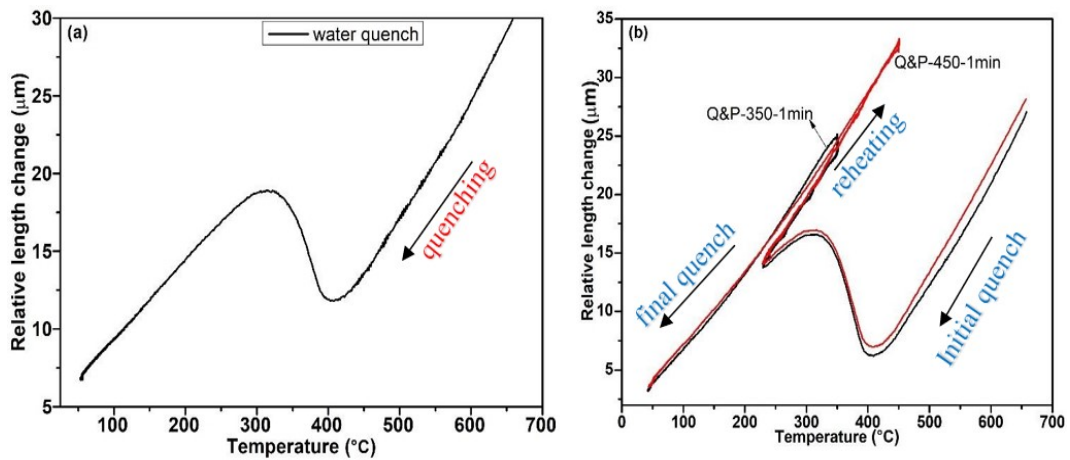


Figure 11: Dilatometer analysis showing the relative length change with respect to temperature in (a) water quenched CMnSiAl specimen, (b) relative change in length during Q&P treatment of (i) initial quenching, (ii) reheating and followed by (iii) final quenching to room temperature in Q&P-350-1min and Q&P-450-1min specimens.

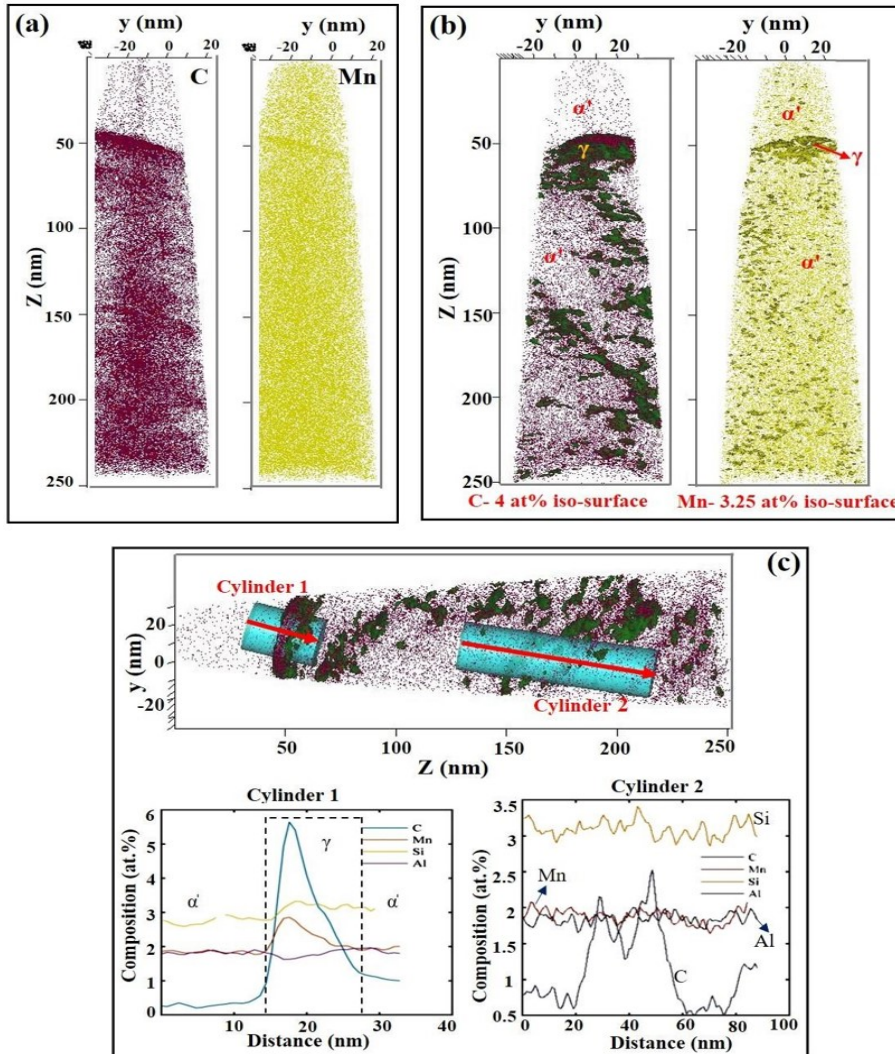


Figure 12: APT analysis of Q&P-350-1min specimen showing (a) the carbon and Mn distribution map in the martensite (α') and austenite (γ); (b) represents 4 at.% carbon iso-surface and the 3.25 at.% Mn iso-surface; (c) shows 1D concentration profile of carbon and the other elemental distribution in the austenite and martensite along interface on the area marked by the red arrows in cylinder 1 and 2, respectively.

of carbides possibly due to tempering of martensite were observed from TEM analysis (Fig. 9 and 10).

The effect of carbon content on paraequilibrium phase boundaries and T_0 temperature was calculated using ThermoCalc software with TCFE9 Gibbs energy database [18] and is shown in Fig. 14. The calculated T_0 temperature (at which both ferrite and austenite have the same Gibbs energy) for the CMnSiAl steel adopted for the current study having 0.26 wt.% C is 703°C (Fig. 14). The selected partitioning temperatures for the current study are well below the calculated T_0 temperature and so only carbon migration is expected to happen during partitioning treatment. But, a slight increase in relative length (0.024 %) was measured during partitioning at 350°C in Q&P-350-1min specimen (Fig. 11b).

During the Q&P treatment, after initial intermediate quenching at 240°C, both martensite and retained austenite contains 0.26 wt.% of carbon as nominal composition of the steel. In order to stabilize the austenite during partitioning at 350°C, the amount of carbon required (γ_C at 350°C as in Fig. 14) is greater than 4 wt.% as per the above paraequilibrium Ae_3 boundary calculation (as marked in Fig. 14) and the carbon content to be enriched from the nominal value is high (i.e., from 0.26 to 4 wt.%). So, during partitioning at 350°C, at initial stage, possibly small migration of martensite-austenite interface takes place until the enrichment of carbon reaches 4 wt.% in austenite, since it is

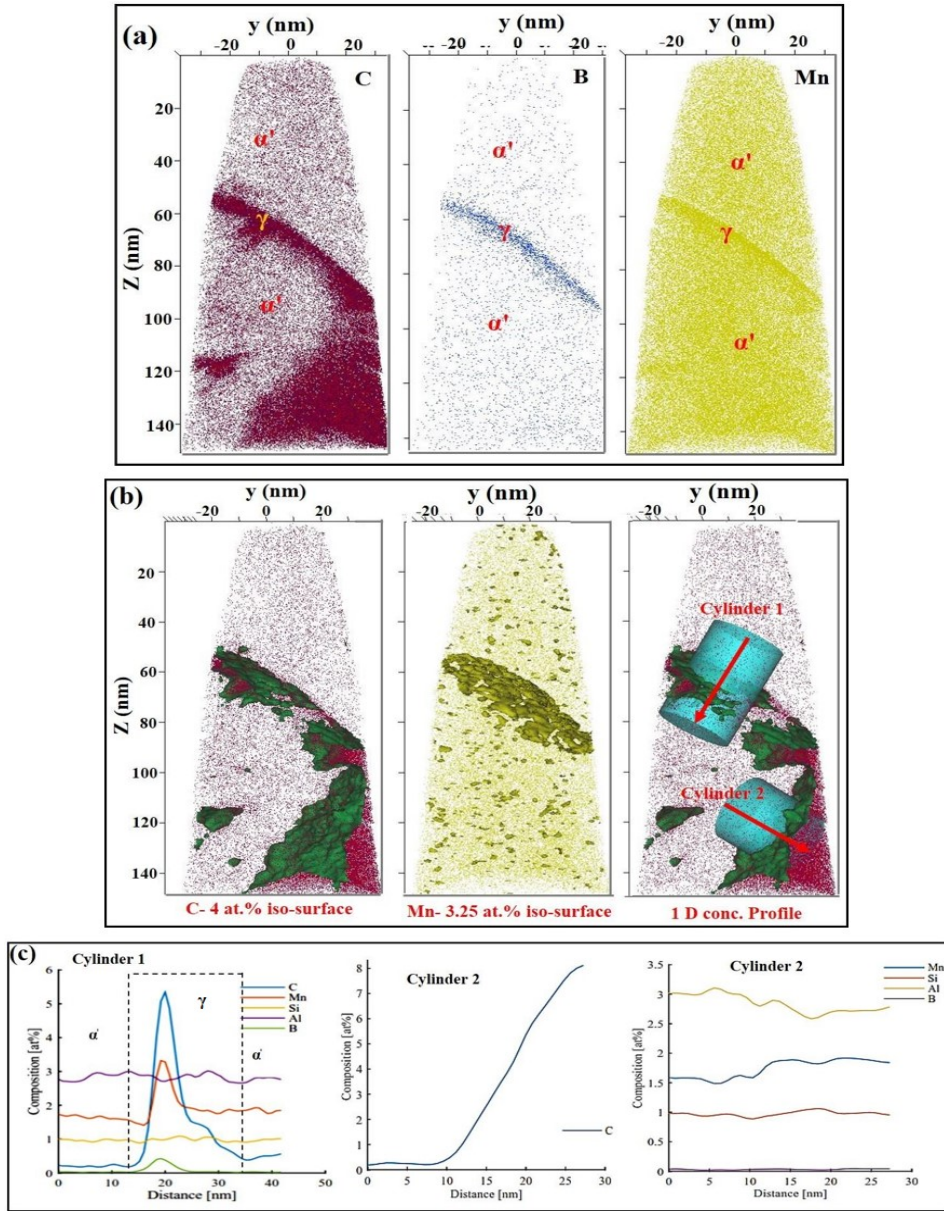


Figure 13: APT analysis of Q&P-450-1min specimen (a) showing the carbon (C), boron (B) and Mn distribution map in the martensite (α') and austenite (γ); (b) represents 4 at.% carbon iso-surface, iso-surface of 3.25 at.% of Mn and 1D concentration profile of carbon; (c) elemental distribution in the austenite and martensite along interface measured in the cylinder1 and cylinder2 along the red arrows as marked in (b).

still within the martensitic transformation zone (between M_S and M_f). This is one of the possible causes for slight expansion that was observed in the specimen that was partitioned at 350°C (Fig.11b). As soon as the austenite carbon content reaches 4 wt.%, only carbon diffusion/partitioning continues during holding at 350°C. Similar expansion was reported by Dai *et al.* [14] as, it is due to the interface migration from martensite into austenite during partitioning in a Fe-C-Mn-Si steel.

Another possibility for the expansion to happen in Q&P-350-1min specimen is, the austenite that was present in between two martensite laths could have transformed isothermally to a fresh martensite during partitioning and may appear as a single thicker lath after transformation. Moreover, if the austenite (FCC) to bainite (BCC) transformation has happened in Q&P-350-1min specimen, the change in dimension of specimen or the expansion should be 0.06%

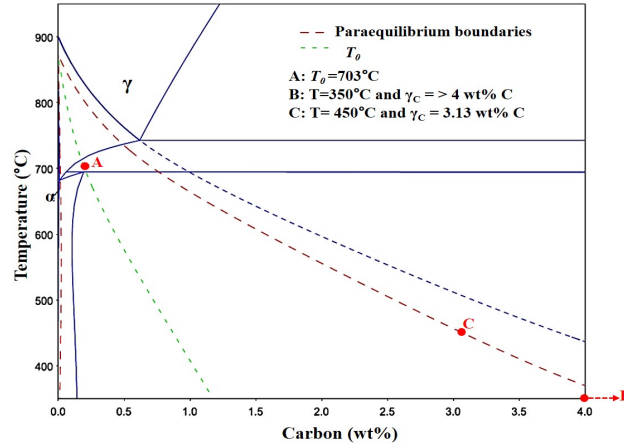


Figure 14: Calculation of paraequilibrium phase boundaries and T_0 temperature variation w.r.t carbon content in the CMnSiAl steel.

[8, 14, 28]. But the observed relative length change is small (0.024%) and so no bainitic transformation could have happened in Q&P-350-1min specimen. Also, no presence of bainite was observed from the TEM analysis (Fig7 and 8) of Q&P-350-1min specimen. Therefore, it could be considered as a slight martensite-austenite interface migration or isothermal martensite formation or cumulative effect of both, that took place during partitioning and led to increase in martensite lath thickness in Q&P-350-1min specimen. Thus, more of the carbon depleted martensite with increase in lath thickness that are formed during initial quenching was observed in the final Q&P microstructure in Q&P-350-1min specimen as compared to Q&P-450-1min specimen (Fig.4).

In case of Q&P-450-1min (above M_S) specimen, the rate of carbon diffusion and carbon diffusion distance (i.e., from interface into the austenite grain or inter-lath film) is expected to be more as compared to 350°C in the same 1 min of partitioning time. Therefore, the enrichment of carbon is expected to happen faster in former case to reach 3.1 wt.% carbon (γ_C at 450°C as in Fig.14) that is required as per the above explained paraequilibrium Ae_3 boundary calculation, as well as for a longer distance in austenite grain or film. So, negligible amount of interface migration or isothermal martensite transformation could have happened and so no significant expansion was observed in case of Q&P-450-1min specimen. Therefore, 2% increase in stabilization of austenite with 0.27 wt.% increase in carbon content (both blocky and interlath austenite) could be achieved finally after the Q&P treatment in case of Q&P-450-1min specimen as compared to Q&P-350-1min specimen. This increase in carbon content in austenite measured from synchrotron XRD measurement and the presence of tempered martensite along with some traces of carbides from TEM analysis strongly supports the partitioning of carbon and tempering effect (i.e., releasing carbon from martensite laths due to partitioning which reduces the stresses that are present in the laths formed during intermediate quenching) that took place during partitioning in Q&P-450-1min specimen. Similar tempering or stress relieving was reported by Speer, *et al.*, in steels partitioned above M_S temperature [8].

Therefore, the above results suggest that, the following are the possible mechanisms that involves during partitioning treatment: The carbon partitioning and interface migration/isothermal martensite formation are the major mechanisms that could happen in case of below M_S partitioned (Q&P-350-1min) specimen. Whereas the carbon partitioning along with tempering in martensite could happen during partitioning above M_S temperature (as in Q&P-450-1min specimen).

4.2. Effect of partitioning temperature on carbon enrichment in austenite

EPMA elemental mapping shows that all the substitutional elements (Mn, Si and Al) were uniformly distributed between the phases throughout the microstructure for Q&P-350-1min specimen (see the supplementary data). However, the APT measurements revealed a slight increase in Mn content (approximately 1 at.% increase from nominal value) locally in an austenite (for 10-15 nm) region as compared to the neighboring martensite in both Q&P-350-1min (Fig.12) and Q&P-450-1min (Fig. 13) specimens. But it is not the case throughout the analyzed region in APT needle, i.e., enrichment of Mn was not always present (in Mn map) wherever the carbon is enriched (as in C- map) (as in cylinder 2 in Fig. 12c and 13c respectively) and there was no microsegregation observed in both Q&P-350-1min and

Q&P-450-1min specimens. Thus, the Mn enrichment in the analyzed region of austenite is due to some local segregation that could have happened during casting itself in both the specimens. A very small variation in silicon (Si) content was observed in austenite in Q&P-350-1min (below M_S partitioning) specimen, which is also due to the casting effect and thus the substitutional elements that are present in CMnSiAl steel are not contributing to the partitioning between the martensite and austenite.

From Fig.12c and 13c it is evident that a significant increase in carbon was observed in the austenite (γ) after partitioning process (center of the peak) for a distance of approximately 10-15nm, which is expected to be the inter-lath retained austenite film in both Q&P-350-1min and Q&P-450-1min specimens. The maximum amount of carbon present in austenite is nearly 1.2 wt.% (5.6 at.%) in both cases of above and below M_S partitioned specimens. If we consider RT (i.e., at 25°C) as the M_S temperature and by fixing the amount of all the substitutional elements as constant (as in the alloy composition of 1.57 Mn- 1.06 Si-0.98 Al (in wt.%)), then the amount of carbon required to stabilize austenite is 1.15 wt.% as per the following equation 3 [6].

$$M_S(^{\circ}C) = 539 - 423C - 30.4Mn - 7.5Si + 30Al \quad (3)$$

where, each alloy content is represented in wt.%.

Thus, the measured carbon (from APT) in austenite in both the Q&P-350-1min and Q&P-450-1min (below and above M_S partitioned) specimens is almost equal to the calculated carbon content that needed to retain austenite at RT (from Eq.3) of 1.15 wt.%. Toji *et al.*[29] has also reported similar carbon content of 5 to 8 at.% in Fe-0.59 wt.% C (2.7 at.% C)-2.0 wt.% Si-2.9 wt.% Mn-0.038 wt.% Al steel during tempering at 400°C for 300 s. However, in our study the similar amount of carbon (5.5-5.7 at.%) could be achieved with just 1 min of partitioning at 350 and 450°C. Also, the observed carbon content in martensite (α') is less (marked as α' at left and right side of the peak as in Fig.12c and 13c) as compared to austenite. Thus, in the current study, it is ensured that the carbon has partitioned efficiently from martensite into austenite during the Q&P treatment and the austenite has stabilized with 1.15 wt.% carbon in it after final quenching in both Q&P-350-1min and Q&P-450-1min specimens. The measured carbon content in cylinder 2 of Q&P-350-1min specimen (Fig. 12c) was only 2-2.5 at% (i.e., 0.45-0.56 wt.%), which is greater than the nominal composition of the steel but less than the carbon present in other austenite (cylinder 1). This low carbon (i.e., less than 1.15 wt.%) austenite might have frozen or arrested by neighboring martensite laths and so not allowed for further fresh martensite transformation after final quenching. From this it is evident that, the carbon distribution in all the inter-lath austenite throughout the microstructure is not uniform. In Q&P- 450-1min specimen, the carbon content measured in cylinder 2 is nearly 8 at% (1.79 wt.%) which is more than the carbon required to stabilize the austenite at room temperature. Thus, this confirms that the increase in partitioning temperature has led to more carbon partitioning in austenite as observed from the XRD measurement, even though there is nonuniformity in distribution between different inter-lath austenite in Q&P-450-1min (above M_S partitioned) specimen. But, if the overall carbon content in all the austenite (i.e., carbon enriched inter-lath regions) measured by APT are averaged then the final value will be less. This supports the measured carbon content from synchrotron XRD (bulk measurement with nearly 2 mm of interaction volume which contains both blocky as well as inter-lath austenite) which is lesser than the APT (localized technique that measures in a tip of nearly 100 nm) measurement in both Q&P-350-1min and Q&P-450-1min specimens.

Therefore, to conclude, effective carbon partitioning has taken place, and the austenite has stabilized at RT in both the partitioned specimens. The increase in partitioning temperature has led to slight increase in carbon content in retained austenite as compared to below M_S partitioned specimen. The partitioning of Mn was not significantly observed throughout the analyzed region and so it is considered as local effect.

5. Conclusion

To understand the effect of temperature on carbon partitioning mechanism, the CMnSiAl steel chosen for the current study was subjected to two-step Q&P process that were partitioned at below and above M_S temperature (Q&P-350-1min and Q&P-450-1min, respectively) and the results are summarized as follows:

1. In both the Q&P specimens, the presence of distorted BCC or pseudo tetragonal martensite structure was evident with two different characteristics namely (i) tempered or partitioned martensite formed during initial quenching ($M_f < 240^{\circ}C < M_S$) and partitioning step (ii) carbon enriched fresh martensite formed after partitioning step and final quenching. Blocky retained austenite and inter-lath retained austenite film in martensite colonies/packets were present in both the Q&P specimens. In addition, packets of M/A constituents were observed in Q&P-350-1min specimen and some traces of carbide and plate martensite were observed in Q&P-450-1min specimen.

2. In addition to carbon partitioning, slight interface mobility/isothermal martensite formation was observed in below M_S partitioned specimen, whereas along with carbon partitioning tempering of martensite also occurred in case of above M_S partitioned specimen.
3. Irrespective of the partitioning temperature, effective carbon partitioning was promoted in the austenite and its stabilization occurred at RT with 1.15 wt.% carbon in both the Q&P specimens. The substitutional elements that are present in the Q&P specimens did not display any significant partitioning, even though some local segregation was observed due to casting.

Acknowledgement

The authors sincerely acknowledge DESY (Deutsches Elektronen-Synchrotron), Hamburg, Germany, for providing the high energy Synchrotron XRD facility and Mr. Ankit kumar from Delft university of Technology, Netherlands for helping in the APT measurements.

N. Maheswari, sincerely thank Indian Institute of Technology Madras (IITM), India and RWTH Aachen University, Germany, for supporting her research stay at RWTH through student exchange program and thanks the Clausthal University of Technology, Germany, for supporting her research stay at Helmholtz-Zentrum Geesthacht, Hamburg, Germany, to carry out high energy Synchrotron XRD analysis. Prof. S. Sankaran thank Alexander Von Humboldt foundation for his research stay in Germany through AvH fellowship for the experienced researchers.

Author contributions

N. Maheswari: Conceptualization, Methodology, Investigation, validation, Formal analysis, Data curation, Visualization, Writing - Original Draft.

Murugaiyan Amirthalingam: Conceptualization, Writing - review & editing.

Alexander Schwedt: Investigation, Writing - review & editing.

Heinz Günter Brokmeier: Resources, Writing - review & editing.

Norbert Schell: Investigation.

Joachim Mayer: Resources, Writing - review & editing.

K.C. Hari Kumar: Software, Investigation, Writing - review & editing.

S. Sankaran: Supervision, Writing - review & editing, Project administration, Funding acquisition.

Appendix A: Supplementary data

Supplementary data can be found here.

Electron probe microanalysis of Q&P-350-1min specimen showing (a) microstructure; (b, c and d) elemental maps of Si, Mn, and Al respectively.

Data availability statement

The raw/processed data required to reproduce these findings cannot be shared at this time as the data also forms part of an ongoing study.

References

- [1] J. Speer, D.K. Matlock, B.C. De Cooman, J.G. Schroth, Carbon partitioning into austenite after martensite transformation, *Acta Materialia*. 51 (2003) 2611–2622. [https://doi.org/10.1016/S1359-6454\(03\)00059-4](https://doi.org/10.1016/S1359-6454(03)00059-4).
- [2] M.J. Santofimia, T. Nguyen-Minh, L. Zhao, R. Petrov, I. Sabirov, J. Sietsma, New low carbon Q&P steels containing film-like intercritical ferrite, *Materials Science and Engineering A*. 527 (2010) 6429–6439. <https://doi.org/10.1016/j.msea.2010.06.083>.
- [3] Z. Cai, D. Tang, H.-T. Jiang, Zhao Song-Shan, Li Hui, Process Simulation and Microstructure Analysis of Low Carbon Si-Mn Quenched and Partitioned Steel, *Journal of Iron and Steel Research International*. 15 (2008) 82–85. [https://doi.org/10.1016/S1006-706X\(08\)60149-1](https://doi.org/10.1016/S1006-706X(08)60149-1).
- [4] E. De Moor, S. Lacroix, A.J. Clarke, J. Penning, J.G. Speer, Effect of retained austenite stabilized via quench and partitioning on the strain hardening of martensitic steels, *Metallurgical and Materials Transactions A: Physical Metallurgy and Materials Science*. 39 (2008) 2586–2595. <https://doi.org/10.1007/s11661-008-9609-z>.
- [5] M.J. Santofimia, L. Zhao, R. Petrov, J. Sietsma, Characterization of the microstructure obtained by the quenching and partitioning process in a low-carbon steel, *Materials Characterization*. 59 (2008) 1758–1764. <https://doi.org/10.1016/j.matchar.2008.04.004>.

- [6] A.J. Clarke, J.G. Speer, M.K. Miller, R.E. Hackenberg, D. V. Edmonds, D.K. Matlock, F.C. Rizzo, K.D. Clarke, E. De Moor, Carbon partitioning to austenite from martensite or bainite during the quench and partition (Q&P) process: A critical assessment, *Acta Materialia*. 56 (2008) 16–22. <https://doi.org/10.1016/j.actamat.2007.08.051>.
- [7] M.J. Santofimia, L. Zhao, R. Petrov, C. Kwakernaak, W.G. Sloof, J. Sietsma, Microstructural development during the quenching and partitioning process in a newly designed low-carbon steel, *Acta Materialia*. 59 (2011) 6059–6068. <https://doi.org/10.1016/j.actamat.2011.06.014>.
- [8] J.G. Speer, E. De Moor, A.J. Clarke, Critical Assessment 7: Quenching and partitioning, *Materials Science and Technology*. 31 (2015) 3–9. <https://doi.org/10.1179/1743284714Y.0000000628>.
- [9] Y. Takahama, M.J. Santofimia, M.G. Mecozzi, L. Zhao, J. Sietsma, Phase field simulation of the carbon redistribution during the quenching and partitioning process in a low-carbon steel, *Acta Materialia*. 60 (2012) 2916–2926. <https://doi.org/10.1016/j.actamat.2012.01.055>.
- [10] M.G. Mecozzi, J. Eiken, M.J. Santofimia, J. Sietsma, Phase field modelling of microstructural evolution during the quenching and partitioning treatment in low-alloy steels, *Computational Materials Science*. 112 (2016) 245–256. <https://doi.org/10.1016/j.commatsci.2015.10.048>.
- [11] N. Maheswari, S.G. Chowdhury, K.C. Hari Kumar, S. Sankaran, Influence of alloying elements on the microstructure evolution and mechanical properties in quenched and partitioned steels, *Materials Science and Engineering A*. 600 (2014) 12–20. <https://doi.org/10.1016/j.msea.2014.01.066>.
- [12] S. Karewar, J. Sietsma, M.J. Santofimia, Effect of C on the martensitic transformation in Fe-C alloys in the presence of pre-existing defects: A molecular dynamics study, *Crystals*. 9 (2019) 1–13. <https://doi.org/10.3390/cryst9020099>.
- [13] A.K. Behera, G.B. Olson, Prediction of Carbon Partitioning and Austenite Stability via Non-equilibrium Thermodynamics in Quench and Partition (Q&P) Steel, *The Minerals, Metals & Materials Society*. 71 (2019) 1375–1385. <https://doi.org/10.1007/s11837-019-03369-z>.
- [14] Z. Dai, R. Ding, Z. Yang, C. Zhang, H. Chen, Elucidating the effect of Mn partitioning on interface migration and carbon partitioning during Quenching and Partitioning of the Fe-C-Mn-Si steels: Modeling and experiments, *Acta Materialia*. 144 (2018) 666–678. <https://doi.org/10.1016/j.actamat.2017.11.025>.
- [15] J.G. Speer, D.K. Matlock, B.C. De Cooman, J.G. Schroth, Comments on “On the definitions of paraequilibrium and orthoequilibrium” by M. Hillert and J. Agren, *Scripta Materialia*, 50, 697–9 (2004), *Scripta Materialia*. 52 (2005) 83–85. <https://doi.org/10.1016/j.scriptamat.2004.08.029>.
- [16] S.S. Babu, E.D. Specht, S.A. David, E. Karapetrova, P. Zschack, M. Peet, H.K.D.H. Bhadeshia, In-situ observations of lattice parameter fluctuations in austenite and transformation to bainite, *Metallurgical and Materials Transactions A: Physical Metallurgy and Materials Science*. 36 (2005) 3281–3289. <https://doi.org/10.1007/s11661-005-0002-x>.
- [17] S. Ebner, C. Suppan, A. Stark, R. Schnitzer, C. Hofer, Austenite decomposition and carbon partitioning during quenching and partitioning heat treatments studied via in-situ X-ray diffraction, *Materials and Design*. 178 (2019) 107862. <https://doi.org/10.1016/j.matdes.2019.107862>.
- [18] Thermo-Calc, (n.d.). www.thermocalc.com.
- [19] M.J. Santofimia, L. Zhao, J. Sietsma, Overview of mechanisms involved during the quenching and partitioning process in steels, *Metallurgical and Materials Transactions A: Physical Metallurgy and Materials Science*. 42 (2011) 3620–3626. <https://doi.org/10.1007/s11661-011-0706-z>.
- [20] P. Suwanpinij, The Synchrotron Radiation for Steel Research, *Advances in Materials Science and Engineering*. 2016 (2016) 1–6. <https://doi.org/10.1155/2016/2479345>.
- [21] H.G. Brokmeier, S.B. Yi, Texture and Texture Analysis, in; *Neutron and Synchrotron Radiation in Engineering Materials Science*, Wiley VCH, Weinheim, Germany, 2008.
- [22] C. Garcia-Mateo, J.A. Jimenez, H.W. Yen, M.K. Miller, L. Morales-Rivas, M. Kuntz, S.P. Ringer, J.R. Yang, F.G. Caballero, Low temperature bainitic ferrite: Evidence of carbon super-saturation and tetragonality, *Acta Materialia*. 91 (2015) 162–173. <https://doi.org/10.1016/j.actamat.2015.03.018>.
- [23] M.J. Santofimia, R.H. Petrov, L. Zhao, J. Sietsma, Microstructural analysis of martensite constituents in quenching and partitioning steels, *Materials Characterization*. 92 (2014) 91–95. <https://doi.org/10.1016/j.matchar.2014.03.003>.
- [24] H. Kitahara, R. Ueki, N. Tsuji, Y. Minamino, Crystallographic features of lath martensite in low-carbon steel, *Acta Materialia*. 54 (2006) 1279–1288. <https://doi.org/10.1016/j.actamat.2005.11.001>.
- [25] A. Bojack, L. Zhao, P.F. Morris, J. Sietsma, Austenite Formation from Martensite in a 13Cr6Ni2Mo Supermartensitic Stainless Steel, *Metallurgical and Materials Transactions A: Physical Metallurgy and Materials Science*. 47 (2016) 1996–2009. <https://doi.org/10.1007/s11661-016-3404-z>.
- [26] V.A. Lobodyuk, Y.Y. Meshkov, E. V. Pereloma, On Tetragonality of the Martensite Crystal Lattice in Steels, *Metallurgical and Materials Transactions A: Physical Metallurgy and Materials Science*. 50 (2019) 97–103. <https://doi.org/10.1007/s11661-018-4999-z>.
- [27] Y. Lu, H. Yu, R.D. Sisson, The effect of carbon content on the c/a ratio of as-quenched martensite in Fe-C alloys, *Materials Science and Engineering A*. 700 (2017) 592–597. <https://doi.org/10.1016/j.msea.2017.05.094>.
- [28] A. Saha Podder, H.K.D.H. Bhadeshia, Thermal stability of austenite retained in bainitic steels, *Materials Science and Engineering A*. 527 (2010) 2121–2128. <https://doi.org/10.1016/j.msea.2009.11.063>.
- [29] Y. Toji, H. Matsuda, M. Herbig, P.P. Choi, D. Raabe, Atomic-scale analysis of carbon partitioning between martensite and austenite by atom probe tomography and correlative transmission electron microscopy, *Acta Materialia*. 65 (2014) 215–228. <https://doi.org/10.1016/j.actamat.2013.10.064>.